NIPPON STEEL TECHNICAL REPORT No. 91 January 2005

UDC 669 . 15' 26' 3 - 155 . 3 : 543 . 5

Three-dimensional Atom Probe Analysis of Nitriding Steel Containing Cr and Cu

Jun TAKAHASHI*1 Kaoru KAWASAKI*2
Kazuto KAWAKAMI*1 Masaaki SUGIYAMA*1

Abstract

Three-dimensional atom probe analysis of very fine precipitates was performed on a soft-nitrided steel containing Cr and Cu. Cu precipitates, Cr nitride precipitates and their pairs, which mainly contribute to hardening due to nitriding, were observed in the surface region of the material, while only Cu precipitates were observed in the inner region. From the investigation on the distribution and morphology of the precipitates, it was found that there are the three stages of precipitation as follows. In the heat treatment for nitriding, Cu precipitates were generated first. Then, Cr nitrides nucleated heterogeneously on the surface of the Cu precipitates and their pairs formed. Finally, single Cr nitrides were nucleated homogeneously.

1. Introduction

Nitriding is a very effective method for hardening the surface portion of a steel material and improving its wear resistance and fatigue resistance, and as such, it is widely employed as a surface improvement technique for automobile steel parts. Carbonizing is another surface improvement technique, but nitriding is superior in terms of thermal strain and size accuracy owing to its lower processing temperature. Through nitriding, a compound layer consisting mainly of iron nitride forms in the outermost portion and a diffusion layer hardened by nitrogen (N) in the portions a little to the inside. The hardening mechanisms of the diffusion layer so far proposed include the solid solution hardening by supersaturated N atoms, the hardening by G.P. zones of alloying elements and N, and that by fine precipitate particles[1-4]. However, there has been no quantitative understanding, and many aspects remain unclear owing to the difficulty in directly observing very fine precipitate particles or solute atoms by conventional analysis methods.

The steel the authors used for the nitriding test herein reported contained Cr and Cu as the alloying elements, and Cu was expected to precipitate by the thermal activation of nitriding treatment in addition to nitrides[5]. For observing the presence, distribution, etc. of the precipitates, the authors analyzed the steel in detail using a three-dimensional atom probe (3D-AP)[6]. The expected formation of two different kinds of precipitates in the steel was of grate interest in relation to hardening and precipitation mechanisms. The object of this paper is to clarify the hardening and precipitation mechanisms in the nitriding steel based on the investigation of the formation behavior, the distribution and morphology of the precipitates.

The 3D-AP is an apparatus having a spatial resolution capacity on an atomic level, capable of three-dimensionally visualizing the spatial distribution of approximately one million atoms of constituent elements of a specimen. The use of an energy compensator and other auxiliary devices has improved the mass resolution capacity of the 3D-AP in its actual application[7,8], and it has become a powerful tool for the nanoscopic structural analysis of metal materials[9]. **Fig. 1** schematically shows the principle of the 3D-AP. A high-voltage DC and pulsating current is applied on a needle-shaped specimen, and a strong electrical field forming on the specimen apex surface causes individual constituent atoms at the surface to ionize and evaporate[10]. The kinds and positions of constituent atoms are determined by measuring the traveling time of ionized atoms to the detector and their landing positions on the detector. The apparatus is capable of analyzing any constituent elements from light elements such as H, B, C

*1 Advanced Technology Research Laboratories

*2 Hirohata R&D Lab.

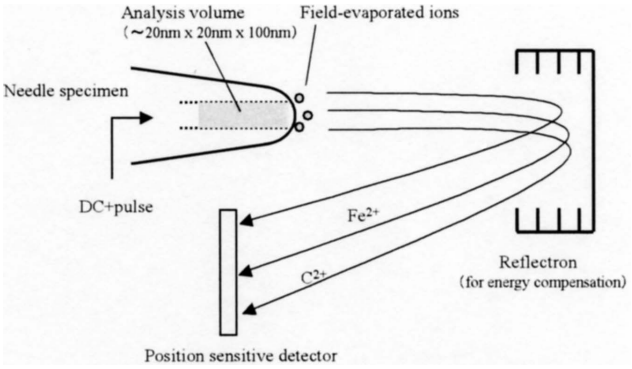

Fig. 1 Schematic drawing of 3D-AP apparatus

and N, which affect the properties of a steel material, to heavy elements. The mass resolution of 3D-AP is so high that it can identify any isotopes of an element.

2. Experimental

The authors used a hot-rolled steel sheet 3 mm in thickness containing mainly 1.0 wt% Cu and 1.3 wt% Cr as a specimen, and subjected it to a soft nitriding treatment in a temperature range of 550 to 600°C for 3 hours in an atmosphere composed of NH_3, N_2, H_2 and CO. A compound layer of iron nitride 15 μm in thickness was found to have formed in the top surface portion. A section of the specimen sheet was polished and the hardness profile in the depth (thickness) direction was measured using a micro-Vickers indenter at a load of 0.1 kg.

Foil specimens for transmission electron microscope (TEM) observation were prepared by cutting out thin sheets from prescribed depths, polishing them into a thickness of 40 μm by chemical polishing and finishing by electropolishing. Needle-shaped specimens for 3D-AP analysis were prepared by cutting out thin sheets from prescribed depths, cutting them into 0.2-mm-square bars, and shaping them into a needle shape having an apex radius of 50 nm or less by the micropolishing technique[11]. A field emission TEM (HF-2000 made by Hitachi Ltd.) operated at 200kV was used for TEM observation and an energy-compensated 3D-AP (made by Oxford Nanoscience Ltd.) for 3D-AP analysis. Atom probe measurements of one million atoms were carried out several times for each specimen under the conditions of a temperature at the specimen position of approximately 70 K, a total probing voltage in the range of 10 to 15 kV, and a pulse fraction of 25%.

3. Experimental Results

3.1 Hardness

While the material hardness of the specimen steel before the nitriding treatment was approximately 100 $HV_{0.1}$, it increased through the treatment to 700 $HV_{0.1}$ or more in the surface layers, and to 200 $HV_{0.1}$ in the inner portion. The specimens for 3D-AP analysis were taken from the depths of 160 μm from the surface where the hardness increase was nearly the largest, 280 μm where the hardness increase was intermediate, and 800 μm as a sample of inner portions where the hardness increase was small. **Table 1** shows the hardness and hardness increment of each of the specimens taken from the above positions.

3.2 TEM observation

Photo 1 shows TEM bright-field images and selected-area dif-

Table 1 Hardness properies of the specimens for 3D-AP

Depth (μm)	Hardness ($HV_{0.1}$)	Increment of hardness ($HV_{0.1}$)
800	201	~100
280	452	~350
160	677	~580

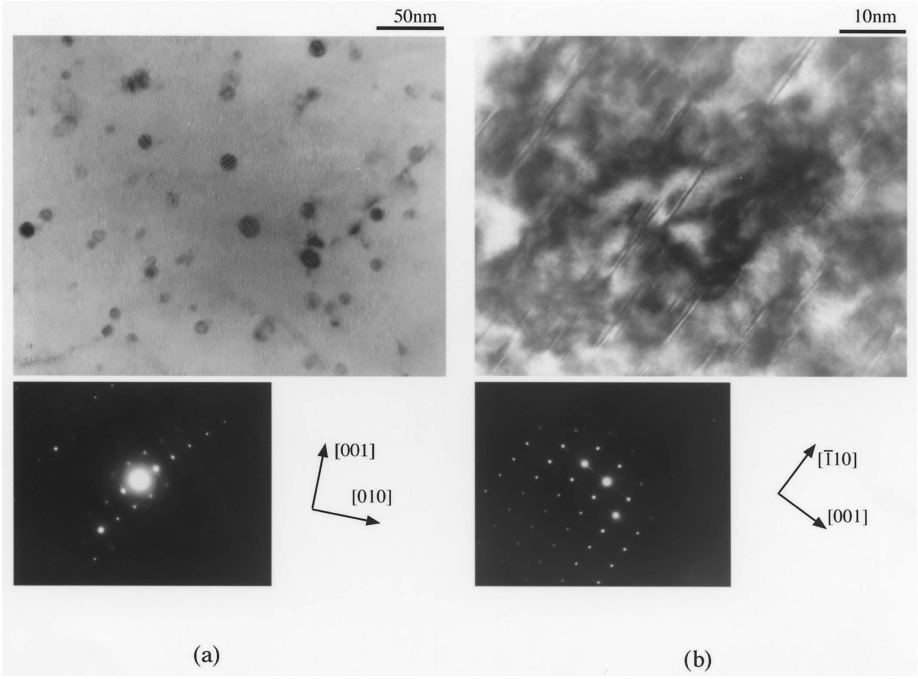

Photo 1 TEM bright-field images and selected area diffract patterns
(a) 800 μm and (b) 160 μm below the surface

fraction (SAD) patterns for the specimens taken from portions 800 and 160 μm in depth (inner and surface portions, respectively). Whereas Cu precipitate particles approximately 20 nm in maximum diameter were observed in a high density in the 800-μm-depth specimen, none of them was observed at al in the 160-μm-depth specimen. Instead, linear structures 6 to 10 nm in length running parallel to the {001} plane were observed in the latter. Diffraction patterns showing distinct streaks extending in the direction perpendicular to the linear structures indicate that they are plate precipitates on the {001} plane. Since the precipitates showed strong strain contrasts, they are most probably nitrides precipitating coherently to the lattice. However, it was impossible to analyze the composition of the precipitates by energy dispersion X-ray spectroscopy (EDS) or to determine the crystal structure by SAD pattern analysis because of their small size.

3.3 3D-AP analysis

A mass-to-charge ratio (m/n) spectrum was obtained from each set of atomic data of 3D-AP analysis, and every ion peak was assigned. Since the specimen steel contained a small amount of Si, which forms Si^{2+} at field evaporation, the Si ions coincided with N^{+} at a m/n of 14 and it was impossible to draw an elemental map of N atoms separately from Si atoms. However, since N atoms concentrated locally at the positions of nitride precipitates, it was possible to analyze the composition of the precipitates. Thus, every ion peak was assigned to an element based on the m/n spectrum, and the results were expressed in the form of three-dimensional (3D) elemental maps.

Fig. 2 shows some 3D elemental maps for a specimen taken from the 800-μm-depth portion representing inner portions. The box size of the maps is shown in the figure. A dot in the map corresponds to an atom. One sees a roughly spherical Cu precipitate approximately 10 nm in diameter in the Cu map. The number density of such Cu particles was estimated at approximately 5×10^{16} cm^{-3} from the number of the Cu particles observed and the volume analyzed. While Cu precipitates 20 nm in diameter were observed with TEM (Photo 1 (a)), the Cu particles measured by 3D-AP were mostly smaller, 10 nm or so in size. This implies that the size of the Cu particles is widely distributed, and most of them are small ones 10 nm or so in size actually. On the other hand, Cr atoms were in solid solution virtually homogeneously as seen in the Cr map, and Cr nitride was not found.

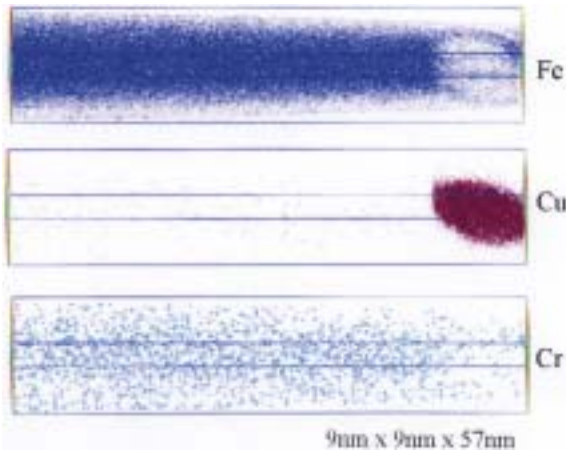

Fig. 2 3D elemental maps of an 800 μm-depth specimen

Fig. 3 shows 3D elemental maps for the specimen taken from the 280-μm-depth portion. Judging from the facts that the distribution of Cr atoms was inhomogeneous forming concentrations locally, that N atoms concentrated at the same locations, and that CrN^{2+} molecular ions (m/n = 31) were observed also at these positions, it is clear that fine Cr nitride precipitates formed. On the other hand, fine Cu particles were also observed, and every one of them was found to form a pair with a Cr nitride precipitate. Observation in more detail revealed clusters composed of Cr and N in regions a little away from the pairs. The number density of Cu particles in this middle depth portion was higher than in the 800-μm-depth (inner) portion, and their size was mostly smaller than 10 nm.

Fig. 4 shows 3D elemental maps for the specimens taken from the 280-μm-depth portion. Here, a map shows two or more elements. In addition to the Cr nitride precipitates that formed pairs with Cu particles seen in Fig. 3, unaccompanied Cr nitride precipitates were

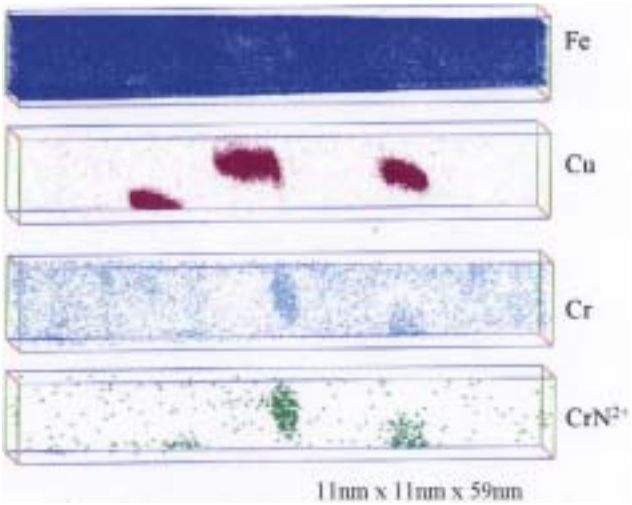

Fig. 3 3D elemental maps of a 280 μm-depth specimen

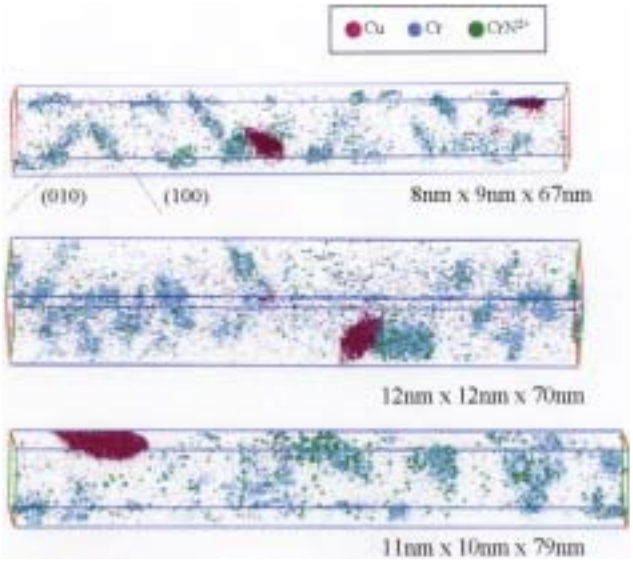

Fig. 4 3D elemental maps of 160 μm-depth specimen

observed in a great number. These Cr nitride precipitates had a plate shape on the {001} plane. The authors noted that the size of the Cr nitride particles forming pairs with Cu particles was apparently larger than that of the unaccompanied Cr nitride particles. What is more, there were regions depleted of precipitates around the pairs.

4. Discussion

4.1 Hardening mechanism

Table 2 shows the size and number density of the precipitates in the specimens obtained through the 3D-AP analysis. The hardening mechanism of the specimen steel presumed from the results is as follows. In the first place, the solid solution hardening due to solute N is inconceivable in the internal portions to which N atoms little diffuse; in fact, the precipitation of Cr nitride was not observed in this portion. This indicates that the hardening in this portion results from the particle hardening (precipitation hardening)[12] by the Cu particles observed in the TEM images of Photo 1 (a) and the 3D elemental maps of Fig. 2. Although Cu particles 20 nm in diameter were found in the TEM observation, what actually contributed to the hardening the most is considered to be the Cu particles 10 nm or so in size that were observed in a high number density in the 3D-AP analysis.

3D-AP analysis at the depth of 160 μm from the surface disclosed that the solute N concentration in regions other than precipitates was approximately 0.5 at%. Based on figures in literatures, the solid solution hardening that this amount of solute N can bring about is estimated at approximately 130 HV[13]. This estimation is much smaller than the actual hardness increment of 580 $HV_{0.1}$ brought about by the nitriding treatment. Therefore, the authors consider that the particle hardening owing to the Cr nitride and Cu particles is mainly responsible for the hardening in the surface portion (N diffusion layer). Since Cu particles always form pairs with Cr nitride particles in the surface portion, the number density of the Cr nitride particles represents that of all the precipitate particles in the portion. Generally, particle hardening depends strongly on the number density of precipitate particles, and for this reason, the Cu particles are considered not to contribute to the material hardening significantly in the surface layers where Cr nitride forms.

The increase in tensile stress when a dislocation is pinned by a particle is expressed by the following equation[12,14]:

$$\Delta\sigma = \left(\frac{\beta G b}{\lambda}\right)\sin\theta \qquad (1)$$

where G is the shear modulus, b is the magnitude of the Burgers vector, λ is the mean particle spacing, θ is the bowing angle between the dislocation line and a straight line that connects two particles, and β is a constant composed of Taylor's factor and the line tension coefficient that changes depending on the magnitude of the stress field around a dislocation, and its value is, admittedly, approximately 3.2[12,14]. In the Orowan mechanism, θ is 90° and the hardness increment becomes the largest under this condition[15]. The 3D-AP measurement can directly calculate particle spacing; the mean spacing between fine Cr nitride particles in the 160-μm-depth portion was estimated at approximately 10 nm from 3D elemental maps.

Assuming that hardness in HV is one-third of tensile stress in MPa[16], the hardness increment in the Orowan mechanism (θ = 90°) is estimated at approximately 2,000 HV. When the estimated hardness increment by solute N (approximately 130 HV) is subtracted from the actual hardness increment of 580 $HV_{0.1}$ shown in Table 1, and the difference of 450 $HV_{0.1}$ is considered to be the hardness increment brought about by particle diffusion hardening, the value of θ calculated from Equation (1) is as small as approximately 13°. This indicates that the cutting mechanism of Cr nitride particles plays an active role. This is presumably because the particles are very fine, they precipitate coherently, and the mean particle spacing is very small.

The conclusion from the above is that the particle hardening with the Cr nitride particles observed in the 3D-AP analysis is dominant in the hardening of the surface portion, and the contribution of iron nitride and the solution hardening by solute N is small.

4.2 Precipitation mechanism

Fig. 5 shows schematic diagrams illustrating the distribution and morphology of the precipitates observed in the present experiment. Whereas Cu precipitates existed unaccompanied in the 800-μm-depth portion, they always formed pairs with Cr nitride particles in the 280- and 160-μm-depth portions. While Cu begins to precipitate at an early stage of nitriding heat treatment, Cr nitride begins to precipitate only after a sufficient amount of N diffuses from the surface. For this reason, Cr nitride is presumed to precipitate using the Cu particles as heterogeneous precipitation nuclei.

In addition to the Cu-Cr nitride pairs, unaccompanied Cr nitride particles were observed in a high density in the 160-μm-depth portion, and they were smaller than the Cr nitride particles that formed the pairs. The above is presumably because the precipitation of the unaccompanied Cr nitride particles started after the Cr nitride particles that formed the pairs started to precipitate. It is likely, therefore, that the Cr nitride that precipitated on the Cu particle surfaces

Table 2 Analysis results of precipitates in the nitriding steel

Depth	CrN precipitate		Cu precipitate	
	Size	Density	Size	Density
(μm)	(nm)	(cm^{-3})	(nm)	(cm^{-3})
800	Not observed		5-20	~5×10^{16}
280	6-8	~1×10^{17}	4-10	~1×10^{17}
160	6-10	~1×10^{18}	4-10	~1×10^{17}

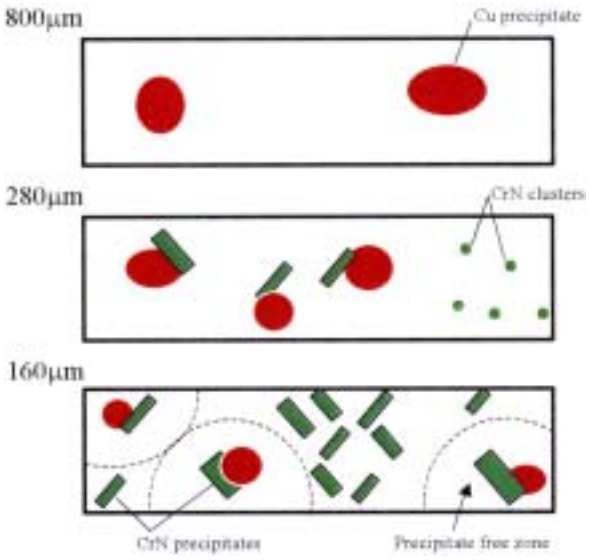

Fig. 5 Schematic diagrams of the distribution of precipitates 800 μm, 280 μm and 160 μm below the surface

absorbed Cr atoms in the neighboring regions during its growth forming the regions depleted of solute Cr, and after N atoms diffused from the surface to this portion to raise the N concentration, new Cr nitride particles formed through homogeneous nucleation in the regions where there was sufficient solute Cr left. The status of this early precipitation is seen as the Cr-N clusters observed in the region 280 μm below the surface. This mechanism explains the formation of the precipitate-depleted regions around the Cu-Cr nitride pairs.

As seen in Table 2, the Cu particles in the surface layers were smaller in size and higher in number density than those in the inner portions. This means that the Ostwald ripening of Cu particles was suppressed in the surface layers for some reason. Judging from the fact that Cu particles in the surface layers always formed pairs with Cr nitride, it is likely that the Fe-Cu interface area of the Cu particles decreased as a result of the pairing, and the interfacial energy, which is the driving force of the Ostwald ripening, decreased as a consequence.

Based on the above discussion, the following three precipitation mechanisms are proposed for the system of the specimen steel. Nitriding heat treatment causes Cu to precipitate in the first place, and then Cr nitride precipitates inhomogeneously using the Cu precipitates as heterogeneous nuclei. Finally, new Cr nitride particles form through homogeneous nucleation in regions away from the already formed Cr nitride particles, where solute Cr is left in a sufficient amount.

5. Conclusion

The authors carried out detail analysis of precipitates in a nitriding steel using a three-dimensional atom probe. The analysis revealed that fine precipitates of Cr nitride and Cu formed in the steel in high densities, and the precipitates contributed to the hardening of the N diffusion layers through particle hardening. The very fine size of the Cr nitride particles and their high number density in the surface layers indicates that the cutting mechanism of the fine precipitates was in operation. The analysis made it clear that the two kinds of precipitate particles formed through three-staged precipitation mechanism during nitriding heat treatment.

References

1) Jack, K.H.: Heat Treatment ’73. The Metals Soc., London, 1975, p.39
2) Takase, T.: Tetsu-to-Hagané. 66, 1423 (1980)
3) Suzuki, S., Naito, K.: Tetsu-to-Hagané. 81, 49 (1995)
4) Ishikawa, N., Shirakami, T., Sato, K., Ishiguro, M., Kabasawa, H., Kuwabara, Y.: Tetsu-to-Hagané. 82, 66 (1996)
5) Kishida, K., Akimoto, O.: Tetsu-to-Hagané. 76, 759 (1990)
6) Takahashi, J., Kawasaki, K., Kawakami, K., Sugiyama, M.: Proceedings of 49th International Field Emission Symposium. Graz, Austria, 2004
7) Sijbrandij, S.J., Cerezo, A., Godfrey, T.J., Smith, G.D.W.: Appl. Surf. Sci. 94/95, 428 (1996)
8) Cerezo, A., Godfrey, T.J., Sijbrandij, S.J., Smith, G.D.W., Warren, P.J.: Rev. Sci. Instrum. 69, 49 (1998)
9) Hono, K.: Prog. Mater. Sci. 47, 621 (2002)
10) Sakai. A.: J. Appl. Phys. 53, 183 (1984)
11) Miller, M.K., Smith, G.D.W.: Atom Probe Microanalysis. Principles and Applications to Materials Problem. Material Research Society, Pittsburgh, 1989, 49p
12) Takagi, S.: The Latest Steel Metallurgy by Precipitation Control. ISIJ, Tokyo, 2001, p. 69
13) Pickering, F.B., Gladman, T.: Iron and Steel Inst. Spec. Rep. No. 81, 1963, p.10
14) Nakajima, K., Nimura, Y., Tsuchiyama, T., Takagi, S.: Tetsu-to-Hagané. 89, 28 (2003)
15) Orowan, E.: Internal Stresses in Metals and Alloys, Inst. Metals, London, 1948, p.451
16) Leslie, W.C.: Met. Trans. 3, 5 (1972)